Dendrosomatic Voltage and Charge Transfer in Rat Neocortical Pyramidal Cells In Vitro

DANIEL ULRICH AND CHRISTIAN STRICKER
Institute of Neuroinformatics, University of Zürich and Federal Institute of Technology, CH-8057 Zurich, Switzerland

Received 21 January 2000; accepted in final form 25 May 2000

Ulrich, Daniel and Christian Stricker. Dendrosomatic voltage and charge transfer in rat neocortical pyramidal cells in vitro. *J Neurophysiol* 84: 1445–1452, 2000. Most excitatory synapses on neocortical pyramidal cells are located on dendrites, which are endowed with a variety of active conductances. The main origin for action potentials is thought to be at the initial segment of the axon, although local regenerative activity can be initiated in the dendrites. The transfer characteristics of synaptic voltage and charge along the dendrite to the soma remains largely unknown, although this is an essential determinant of neural input-output transformations. Here we perform dual whole-cell recordings from layer V pyramidal cells in slices from somatosensory cortex of juvenile rats. Steady-state and sinusoidal current injections are applied to characterize the voltage transfer characteristics of the apical dendrite under resting conditions. Furthermore, dendrosomatic charge and voltage transfer are determined by mimicking synapses via dynamic current-clamping. We find that around rest, the dendrite behaves like a linear cable. The cutoff frequency for somatopetal current transfer is around 4 Hz, i.e., synaptic inputs are heavily low-pass filtered. In agreement with linearity, transfer resistances are reciprocal in opposite directions, and the centroids of the synaptic time course are on the order of the membrane time constant. Transfer of excitatory postsynaptic potential (EPSP) charge, but not peak amplitude, is positively correlated with membrane potential. We conclude that the integrative properties of dendrites in infragranular neocortical pyramidal cells appear to be linear near resting membrane potential. However, at polarized potentials charge transferred is voltage-dependent with a loss of charge at hyperpolarized and a gain of charge at depolarized potentials.

INTRODUCTION

Neocortical pyramidal cells receive the majority of excitatory synaptic input onto their dendrites (DeFelipe and Fariñas 1992). A variety of active conductances have been found in dendritic recordings (Amitai et al. 1993; Huguenard et al. 1988; Kim and Connors 1993) and these are likely to influence the propagation of synaptic signals to the soma (Deisz et al. 1991; Markram and Sakmann 1994; Schwindt and Crill 1998; Stafstrom et al. 1985; Stuart and Sakmann 1994, 1995). Sodium-dependent action potential generation is thought to occur mainly at the axon hillock (Stuart and Sakmann 1994). Knowledge of the relationship between synaptic input and spike output in individual neurons is essential for theories of cortical circuits (e.g., Douglas et al. 1995). The size of current flow at the soma after stimulation of dendritic synapses has been estimated under steady-state conditions, involving a large and unknown number of synaptic contacts (Ahmed et al. 1998; Schwindt and Crill 1996). However, the exact contribution of individual synapses to current arriving at the soma remains largely unknown. While passive dendrites are expected to act as low-pass filters, active dendritic properties may either boost or attenuate certain signal components. This could potentially lead to a complex relationship between neural input and output. In these experiments, we use an experimental design that circumvents the stochastic nature of transmitter release. We mimic a synaptic conductance on the apical dendrite with a dynamic current-clamp and measure somatic voltage and charge with a second electrode at the soma. This allows us to quantitatively correlate simulated synaptic input with the current arriving at the soma.

METHODS

Sprague-Dawley rats of either sex (P12–P18) were killed by decapitation. Individual cerebral hemispheres were glued on a stage tilted forward by 15°. Parasagittal slices of 300-μm thickness were cut on a Vibratome (TPI, St. Louis, MI) and incubated at 34°C. Slices were transferred to a recording chamber and superfused at room temperature with standard artificial cerebrospinal fluid containing (in mM) 125 NaCl, 1.25 NaH_2PO_4, 25 $NaHCO_3$, 2.5 KCl, 1 $MgCl_2$, 2 $CaCl_2$, 10 glucose, pH adjusted to 7.4 with 5% CO_2-95% O_2.

Patch pipettes were pulled from thick-walled borosilicate glass (Hilgenberg, Malsfeld, Germany) and filled with a solution containing (in mM) 125 K-gluconate, 5 KCl, 1 $MgCl_2$, 1 $CaCl_2$, 10 HEPES, 11 EGTA; osmolarity 280 mOsmol, pH 7.2 adjusted with KOH. Pipettes used for somatic or dendritic recordings had a tip resistance of about 5 and 15 MΩ, respectively. Pyramidal cells in layer V of somatosensory cortex were visualized with infrared differential interference contrast video microscopy (Dodt and Zieglgänsberger 1990).

Time-varying sinusoids of a linearly increasing frequency (chirps) with 20 pA peak-to-peak amplitude, I_0, were generated digitally between 0.1 and 20 Hz (Hutcheon et al. 1996). The frequency was varied at eight octaves per second. The implementation is such that the instantaneous frequency, ν, of the chirp starts at time $t = 0$, increases linearly with time, and covers the range between the initial frequency ν_0 and the final frequency ν_1, i.e.

$$\nu(t) = \nu_0 + \frac{\nu_1 - \nu_0}{t_1} t$$

Therefore the angle that must be supplied to the electrode is

Present address and address for reprint requests: D. Ulrich, Dept. of Physiology, University of Bern, Bühlplatz 5, CH-3012 Bern, Switzerland (E-mail: Ulrich@pyl.unibe.ch).

The costs of publication of this article were defrayed in part by the payment of page charges. The article must therefore be hereby marked "*advertisement*" in accordance with 18 U.S.C. Section 1734 solely to indicate this fact.

$$2\pi\nu t = 2\pi \int_{t_0=0}^{t_1} \left(\nu_0 + \frac{\nu_1 - \nu_0}{t_1} \mathrm{t} \right) \mathrm{d}t = 2\pi \left(\nu_0 t + \frac{\nu_1 - \nu_0}{2t_1} t^2 + C \right)$$

where C contains information on the phase lag. For zero phase lag, the current amplitude, I, of the chirp then takes the form

$$I = I_0 \cos \left[2\pi \left(\nu_0 + \frac{\nu_1 - \nu_0}{2t_1} t \right) t \right]$$

A dynamic current-clamp (Robinson and Kawai 1993; Sharp et al. 1993) was applied through an Axoclamp 2B amplifier (Axon Instruments, Foster City, CA) in bridge mode via a Labmaster A/D converter (Scientific Solutions, Solon, OH) as described previously (Ulrich and Huguenard 1996, 1997). The effects of electrode resistance and capacitance were minimized by electronic compensation. Due to the fast rise times of excitatory synaptic conductances, AD/DA conversions were executed at up to 25 kHz. Synaptic current was calculated from the dynamic current-clamp protocol. To avoid contamination by high-frequency noise, voltage traces were low-pass filtered with a custom-made eight-pole Bessel filter (design JCSMR-ANU, Australia) at 2 kHz, i.e., well below the limits given by the sampling theorem. A liquid junction potential of −8 mV was subtracted offline.

Time centroids of current or voltage transients were calculated from the first and zeroth moments of current and voltage records as described by Agmon-Snir and Segev (1993). Data are presented as mean ± SE and "n" designates the number of recordings.

RESULTS

Dual whole-cell recordings were obtained from large layer V pyramidal cells in rat somatosensory cortex to characterize voltage and charge transfer from the dendrite to the soma and vice versa. Figure 1*A* shows an example of simultaneous recordings with somatic and dendritic patch electrodes separated by 200 μm. The average dendritic recording distance from the soma was 112 ± 14 μm. All cells were of the regular spiking type (Connors and Gutnick 1990) and had a mean resting membrane potential at the soma of −62 ± 1.5 mV (n = 12). In a linear system, charge transfer and steady-state voltage decay are equal in opposite directions (Carnevale and Johnston 1982; Rall and Segev 1985). Therefore we first investigated the spread of somatic voltage into the dendrite. At rest, small hyperpolarizing current steps were injected into the soma and the membrane voltage deflections were recorded simultaneously by the somatic and dendritic patch electrodes (Fig. 1*B*). As previously shown in layer V pyramids, an apparent sag in membrane voltage was revealed for hyperpolarizing voltage transients at both recording sites (Fig. 1*B*, Stuart and Spruston 1998) and was even more pronounced in the dendrite. The mean somatofugal steady-state voltage transfer ratio (k_{12}) was 0.75 ± 0.03 (n = 9; note that k_{12} is the reciprocal of attenuation). In a passive neuron, k_{12} is expected to decrease with electrotonic distance (X). We calculated the length constant (λ) of the proximal apical dendrite as $\lambda = \sqrt{[(d/4) \cdot (R_m/R_i)]}$ with an axial resistivity (R_i) of 100 Ωcm (Stuart and Spruston 1998) and $R_m = \tau_m/C_m$. The membrane time constant (τ_m) was estimated from fitting an exponential function to the late part of the current step response at the soma (Holmes et al. 1992; data not shown). The average τ_m was 30 ± 3.6 ms. The specific membrane capacitance (C_m) was taken as 1 μF cm^{-2} (Curtis and Cole 1938). Figure 1*C* shows a scatter plot of k_{12} versus the electrotonic distance (X) of the two recording electrodes.

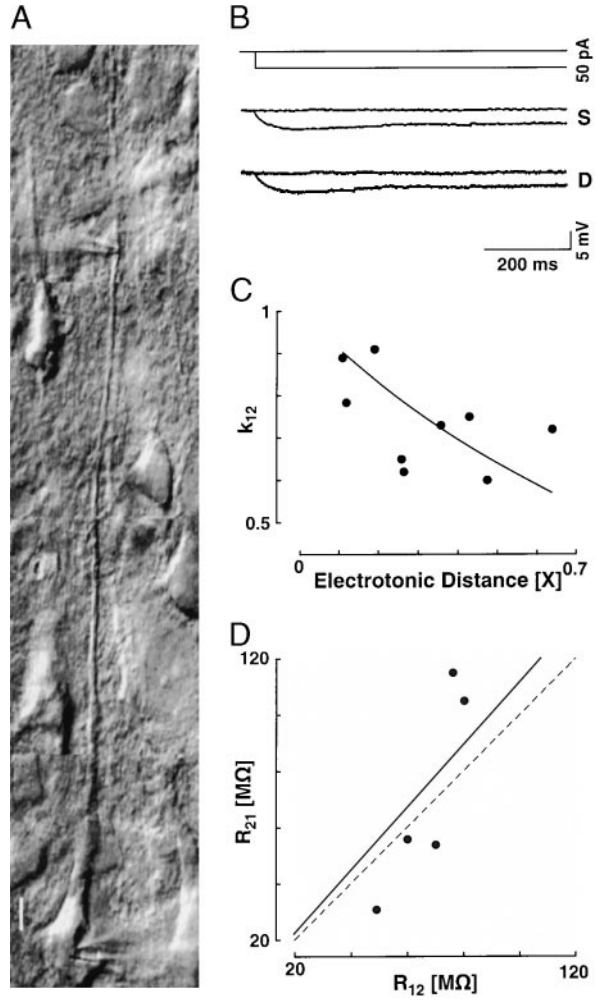

FIG. 1. Somatodendritic steady-state voltage transfer. *A*: composite infrared videomicrograph of a layer V pyramidal cell in rat somatosensory cortex. A patch electrode is positioned at the apical dendrite and another electrode records from the soma. Scale bar corresponds to 10 μm. *B*: somatic current steps (*top trace*) and somatic (*middle*, S) and dendritic (*bottom*, D) voltage recordings were used to estimate the membrane time constant, the input resistance, and the somatofugal steady-state voltage transfer (k_{12}). *C*: scatter plot of k_{12} versus the electrotonic interelectrode distance. The fitted line predicts the voltage profile in a homogeneous equivalent cylinder of electrotonic length 1.7 with a sealed end. *D*: somatofugal transfer resistances (R_{12}) were obtained from data as in Fig. 1*B* and are plotted against their corresponding dendrosomatic values (R_{21}) extrapolated from the chirps (cf. Fig. 2). The straight line was fitted by linear regression through the origin (Pearson's r = 0.89, $P < 0.05$). The (dashed) identity line is shown for reference.

As predicted, dendritic voltage deflections decrease with distance. In Fig. 1*C* the function {cosh ($L - X$)/cosh (L)} was fitted to the data points by a least-squares algorithm. This formula describes the DC voltage decay in a uniform equivalent cylinder of electrotonic length L with a sealed end. The electrotonic length obtained from the fit (L = 1.7) is in agreement with previous estimates of L for the apical dendrite of layer V pyramidal cells based on morphological data (Larkman et al. 1992).

The amplitude ratio between voltage and current at two different sites equals their transfer resistance (R). Figure 1*D* shows a scatter plot of somatofugal transfer resistances (R_{12}) obtained from somatic current injections and corresponding dendrosomatic transfer resistances (R_{21}). The latter were ob-

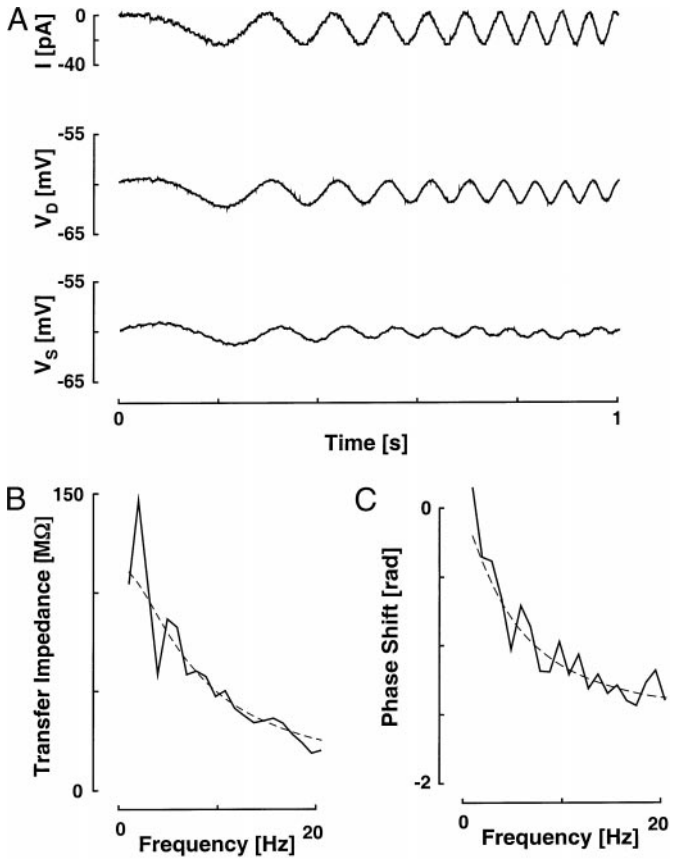

FIG. 2. Frequency dependence of dendrosomatic voltage transfer. *A*: a frequency-modulated sinusoidal current (chirp) was injected into the cell through the dendritic electrode. The resulting membrane voltage oscillations were recorded at the dendrite (V_D) and the soma (V_S). Transfer impedance (*B*) and phase shift (C) in frequency domain were obtained from a single, representative example. An equivalent cable with sealed ends was fitted to the data points by a least-squares algorithm. The parameters of the model cable for this cell are $\tau = 32$ ms, $\lambda = 801$ μm, $l = 1{,}160$ μm, $d = 710$ μm, $x = 450$ μm, and $r = 2.1$ GΩ/cm. Given this value for r and assuming an R_i of 100 Ωcm, a diameter of 2.5 μm for the equivalent cable can be calculated (cf. text for details).

tained from fitting an RC circuit to the chirp data by a least-squares algorithm and extrapolating the fit to DC. Note that at rest, transfer resistances in somatofugal and dendrosomatic directions are highly correlated as shown by the linear fit in Fig. 1*D* (Pearson's $r = 0.89$, $P < 0.05$). Reciprocity of transfer resistances is to be expected in a linear system.

Frequency-dependent voltage transfer from the dendrite to the soma was investigated by sinusoidal current injections through the dendritic electrode (Fig. 2*A*). The resulting voltage was recorded simultaneously by the dendritic and somatic pipettes at resting membrane potential (Fig. 2*A*). Figure 2, *B* and *C*, shows an example of transfer impedance and phase shift between dendritic current and somatic voltage after fast Fourier transformation. The data points were fitted by an equivalent cable with sealed ends (Butz and Cowan 1974): $V(f) = I(f) \cdot Z(\gamma) \cdot \cosh(\gamma x) \cdot \cosh\{\gamma(l - d)\}/\sinh(\gamma l)$. $V(f)$ and $I(f)$ are the Fourier transforms of somatic voltage and dendritic current, and f indicates the frequency. $Z(\gamma)$ and l are the input impedance and length of the equivalent cable, respectively. The relative positions of the recording (x) and stimulation (d) electrodes require that $0 < x < d < l$. The propagation constant (γ) depends on λ and τ: $\gamma = \sqrt{\{(2\pi i f\tau + 1)/\lambda\}}$ and $Z(\gamma)$ is defined as $Z = r/\tau$, where r corresponds to the axial resistance of the cable. The model was fitted to the complex numbers by a least-squares algorithm. The resulting τ and λ from five different cells were 30 ± 4 ms and 400 ± 112 μm. The average length and diameter of the cable are 1169 ± 131 and 2 ± 0.5 μm, respectively. The fitted function in Fig. 2, *B* and *C*, falls monotonically for increasing frequencies. The inflection point is at 4 Hz and coincides approximately with the -3 dB point (5.3 Hz). The maximal initial roll-off is -17 dB per decade, which approaches -10 dB per decade at higher frequencies. Therefore at rest, transient synaptic input will be low-pass filtered by the dendritic cable properties.

Contrary to simple current injections, real synaptic inputs are generated by transmembrane conductances. The resulting current flow is a nonlinear function of the membrane potential. Experimentally, membrane conductances can be mimicked by a hybrid computer system, a dynamic current-clamp. Control experiments were carried out to show that the current generated by the conductance imposed at the soma corresponds to the current that was recovered under voltage-clamp conditions with a second electrode. Double somatic recordings ($n = 4$) were performed on thick-tufted layer V pyramidal cells as illustrated in Fig. 3*A*. With one electrode in current-clamp and the bridge balanced, the conductance time course was imposed. A second electrode in voltage-clamp measured the actual cur-

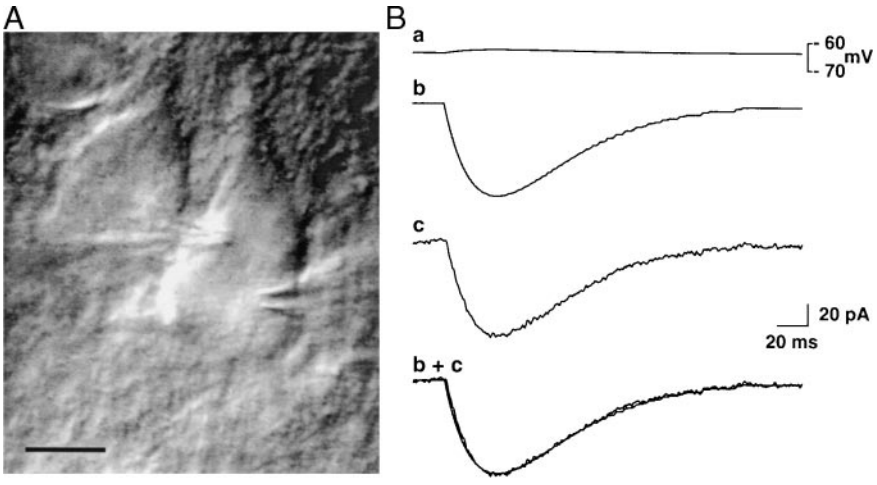

FIG. 3. Recovering the current resulting from a conductance change by voltage-clamp with a second electrode. *A*: experimental arrangement of paired somatic recordings. One electrode is in current-clamp, the other in voltage-clamp mode. The scale bar corresponds to 10 μm. *B*: *top* (*a*) indicates the membrane voltage measured by the electrode in current-clamp with the bridge balanced. The time course of the conductance corresponded to an α-function ($\alpha = 30$) with a reversal potential of 0 mV and an amplitude of 2 nS. The resting membrane potential was -63 mV, which was equivalent to the command potential of the voltage-clamp. The second trace (*b*) is the current passed through the electrode in current-clamp and the third (*c*) is the current recovered by the voltage-clamp electrode. *Bottom*, the two current traces are superimposed ($b + c$).

rent delivered. Such an experiment is shown in Fig. 3*B*, where the conductance time course corresponded to an α-function with $\alpha = 30$, an amplitude of 2 nS, and a reversal potential of 0 mV. The top trace (*a*) is the membrane potential as measured by the electrode in current-clamp. The command potential of the second electrode was set at the resting membrane potential of this cell (−63 mV). At the peak of the conductance, a voltage escape of 1.5 mV was measured. The second trace (*b*) illustrates the current that passed through the electrode in current-clamp. Note the step-like increments in the tail of the excitatory postsynaptic current (EPSC) that are due to the finite resolution achieved with the analog-to-digital converter board. The third time course (*c*) is the current measured by the voltage-clamp electrode. Bottom trace, the two current time courses are superimposed (*b* + *c*). The figure indicates an excellent match between the two currents, except for a small lag during the rising phase (0.7 ms). This is due to incomplete compensation of the series resistance and neutralization of the electrode capacitance.

To estimate the charge arriving at the soma, the cell should be kept in voltage-clamp. However, somatic voltage-clamp would artificially force the membrane potential of the apical dendrite to stay near the command potential and would affect voltage-dependent conductances. As an approximation for the charge arriving at the soma under unclamped conditions, the somatic voltage integral can be divided by the somatic input resistance obtained by linear regression of current-voltage data similar to Fig. 1*B* (not shown). To validate this approach, we compared the charge delivered by the dynamic current-clamp electrode with the estimated charge of the voltage integral scaled by R_N (Fig. 4*A*). In a series of six experiments, double somatic recordings as in Fig. 3*A* were obtained in current-clamp. In each case the membrane potential was held at around −70 mV to provide an equal driving force for the conductance in each of the cells. A dynamic current-clamp was imposed with the second electrode simulating a conductance time course using α-functions of different values (30, 200, 500, 1,000) and a magnitude of 2 nS. In Fig. 4*A*, the scaled voltage integral is plotted against the effective charge delivered through feedback from the dynamic current-clamp. The dashed line indicates equality in charge. The solid line is the linear regression forced through zero with a slope of 1.01 ± 0.01 and a Pearson's $r = 0.996$ ($P < 0.001$). This suggests that for double somatic recordings the somatic charge can be inferred from the scaled voltage integral with excellent accuracy. The scatter in the ordinate for values of $\alpha = 30$ is largely due to the spontaneous synaptic activity encountered in these cells, whereas the scatter in the abscissa is due to the inaccuracy of holding the cell at −70 mV in current clamp.

In a further set of control experiments, we checked if membrane potential affects input resistance (R_N) in layer V pyramidal cells. In Fig. 4*B*, R_N is plotted as a function of membrane potential from three cells of similar input resistance. The result shows a significant linear correlation of R_N with membrane potential, having a slope of 4.8 ± 0.7 MΩ per mV polarization (Pearson's $r = 0.89$, $P < 0.005$). Therefore because the scaled voltage integral as a predictor of charge arriving at the soma is multiplied by ($1/R_N$), it is expected that with depolarization the actual charge is progressively underestimated (cf. Fig. 6*C* and the last paragraph of this section).

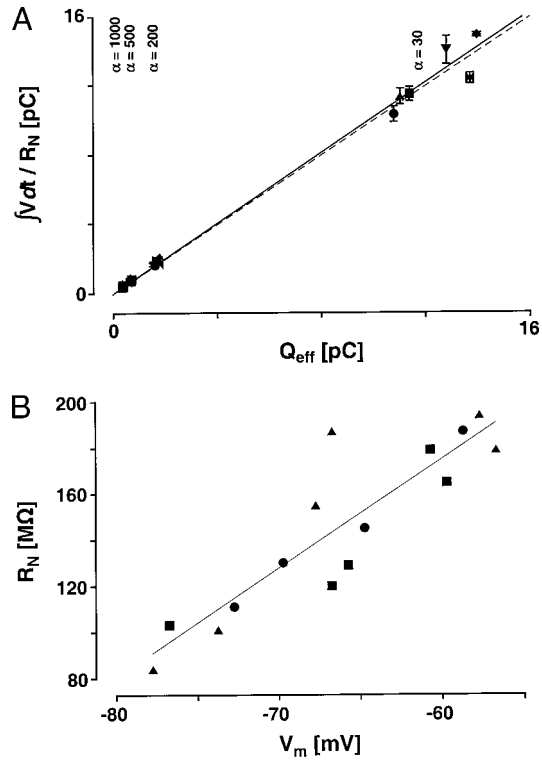

FIG. 4. Assessment of excitaory postsynaptic potential (EPSP) charge estimates at the soma. *A*: scatter plot of charge calculated using the voltage integral divided by input resistance (R_N) versus the effective charge (Q_{eff}) based on the current injected during the dynamic current-clamp. The graph is based on measurements obtained from double somatic patch recordings from 6 cells as in Fig. 3. However, the cells were kept in current-clamp and V_m was held around −70 mV. For simplicity, α-functions of different values (α = 30, 200, 500, 1,000) were used to model the synaptic conductances of 2 nS in each cell (symbol coded). Note that for values of $\alpha = 200$ to 1,000, the 6 data points per α-value overlap to form a single point. The error bars reflect the uncertainty with which R_N could be determined. The dashed line is the prediction of equality. The solid line indicates the linear regression to the data forced through zero with a slope of 1.01 ± 0.01 (Pearson's $r = 0.996$; $P < 0.001$). This line is not different from the line of equality. *B*: input resistance as a function of membrane potential. Scatter plot of the data from 3 cells with comparable R_N (symbol coded). A linear regression of the data revealed that R_N changed at 4.8 ± 0.7 MΩ per mV polarization (Pearson's $r = 0.89$; $P < 0.005$).

To quantify synaptic voltage and charge transfer from dendrite to soma, a dynamic current-clamp was applied to the dendritic pipette. The kinetics of the conductance waveforms were described by two exponential functions with time constants characteristic for fast glutamatergic or GABAergic synapses ($\tau_{rise} = 0.2$ ms, $\tau_{decay} = 1.5$ ms and $\tau_{rise} = 0.4$ ms, $\tau_{decay} = 7.5$ ms, respectively). Peak conductance was varied between 1 and a few nS in agreement with estimates of quantal size (Forti et al. 1997; Stricker et al. 1996). The corresponding (uncorrected) reversal potentials were 0 mV for the EPSC and −65 mV for the inhibitory postsynaptic current (IPSC). Figure 5*A* shows an example of a dendritic dynamic current-clamp EPSP that was simultaneously recorded at the soma. Figure 5*B* depicts another experiment simulating an inhibitory postsynaptic potential (IPSP). Because the driving force for the IPSC is only a few millivolts at rest, the amplitude of the dendritic IPSP is relatively small. EPSP charge transfer and amplitude ratios for EPSPs and IPSPs are summarized in Fig. 5*C*. As expected in a linear system (Carnevale and Johnston 1982; Rall

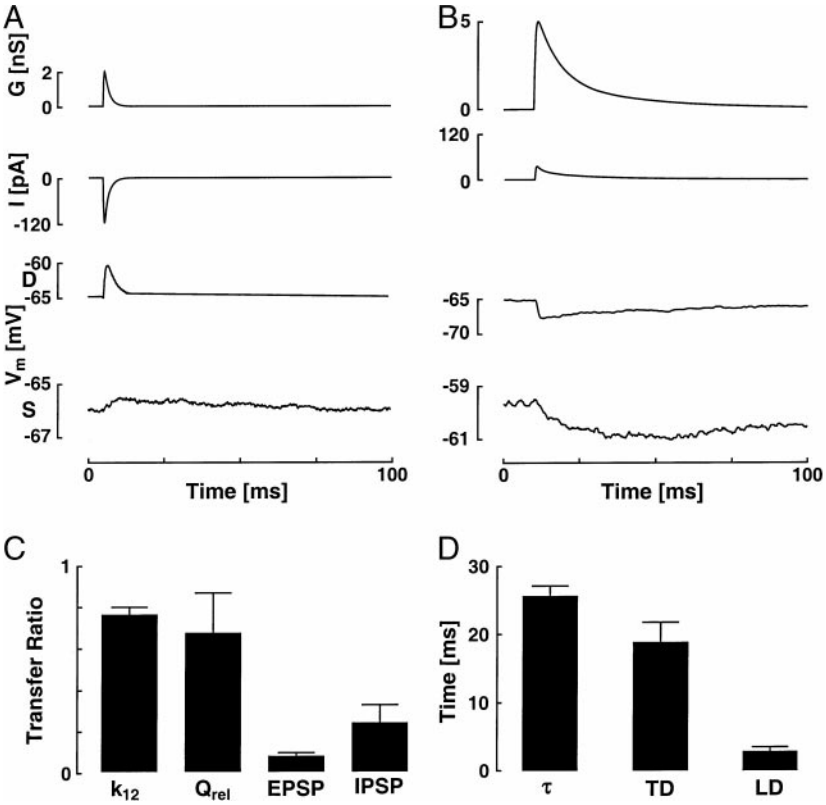

FIG. 5. Synaptic voltage and charge transfer. *A*: excitatory conductance. The synaptic current (second trace) follows the time course of the conductance waveform (upper trace). Dynamic current-clamp EPSP generated at the dendrite (D) and simultaneously recorded at the soma (S). *B*: similar experiment as in *A* but with an inhibitory conductance. Note the small amplitude of the IPSP due to a much smaller driving force than in *A* (few millivolts at rest). *C*: histogram of pooled data of k_{12}, Q_{rel} (EPSP charge ratio), and EPSP and inhibitory postsynaptic potential (IPSP) peak-amplitude transfer ratio. k_{12} and Q_{rel} were not significantly different from each other ($P > 0.05$, paired *t*-test). *D*: histogram of pooled data of the total delay (TD) and local delay (LD) of the EPSP in relation to the membrane time constant (τ). τ and TD were not significantly different from each other ($P > 0.05$, paired *t*-test).

and Segev 1985), dendritic charge transfer at rest is on average comparable to somatodendritic steady-state voltage transfer (Fig. 5*C*). Due to the high-frequency components of a glutamatergic conductance, EPSP amplitude at the soma is significantly reduced (7.7 ± 1.5%, $n = 7$) compared with the EPSP at the input site. Because of the slower time course of the conductance, the IPSP peak amplitudes are reduced less (to about a quarter of the initial size, i.e., 27 ± 7%, $n = 4$). Note that, although data from different experiments are pooled in Fig. 5, *C* and *D*, comparisons were made by a Student's paired *t*-test, i.e., data from individual experiments were compared.

Neuronal integration not only depends on amplitude transfer but also on propagation times (Agmon-Snir and Segev 1993). We determined the time centroids of dendritic EPSC/Ps and of the resulting somatic EPSPs by the method of moments. The centroid delay of synaptic EPSC and EPSP is called the local delay, whereas the time interval between the centroids of somatic EPSP and dendritic EPSC is termed the total delay. Figure 5*D* shows a summary histogram of calculated local and total delays in relation to the membrane time constant. As predicted for a passive neuron, the total delay of dendritic EPSPs was not significantly different from the corresponding membrane time constant. The local delay (2.7 ± 0.5 ms), which determines the integration time at the synapse, was on the order of a tenth of the membrane time constant, again in agreement with simulations of pyramidal cells with passive membrane properties (Fig. 5*D*, cf. Agmon-Snir and Segev 1993).

Various voltage-dependent membrane conductances can be activated by small voltage deflections from rest. Therefore the influence of membrane potential changes on dynamic current-clamp EPSP amplitude and charge transfer was assessed. Dendritic and somatic membrane voltages were simultaneously shifted by DC current injections. Figure 6*A* shows an example of simultaneously recorded somatic and dendritic dynamic current-clamp EPSPs at three different holding potentials (−56, −71, and −78 mV at the soma; single traces). There is a small scatter in membrane voltage between soma and dendrite due to the inability to perfectly clamp the membrane potential in current-clamp mode. As expected, the dendritic EPSP amplitude is diminished with depolarization due to a reduced driving force. At the same time, the somatic EPSP became prolonged. Figure 6, *B* and *C*, show scatter plots of pooled data ($n = 5$; results of each cell symbol coded). While the EPSP peak amplitude ratio was independent of the membrane potential (Fig. 6*B*), charge transfer was strongly voltage-dependent (Fig. 6*C*). Incomplete series resistance and electrode capacitance compensation and variable dendritic seal resistances from experiment to experiment may have contributed to the scatter of the data points in Fig. 6*C*. However, these cannot explain the significant linear relationship between membrane potential and charge transfer (Pearson's $r = 0.44$, $P < 0.04$), which results in a relative charge gain of 30 ± 13% for 10 mV of depolarization. Due to the voltage dependence of R_N, the actual charge gain is expected to be more pronounced, i.e., our estimate is conservative. We recalculated the estimates in Fig. 6*C* for R_N at different holding potentials. The new estimates are still fitted best with a line, but one with an increased slope of 51 ± 15% per 10 mV polarization (Pearson's $r = 0.59$; $P < 0.01$). With respect to charge transfer under passive conditions (horizontal dashed line in Fig. 5*C*), a disproportional loss of charge is found below rest, and a gain of charge between rest and spike threshold (vertical dashed line in Fig. 6*C*).

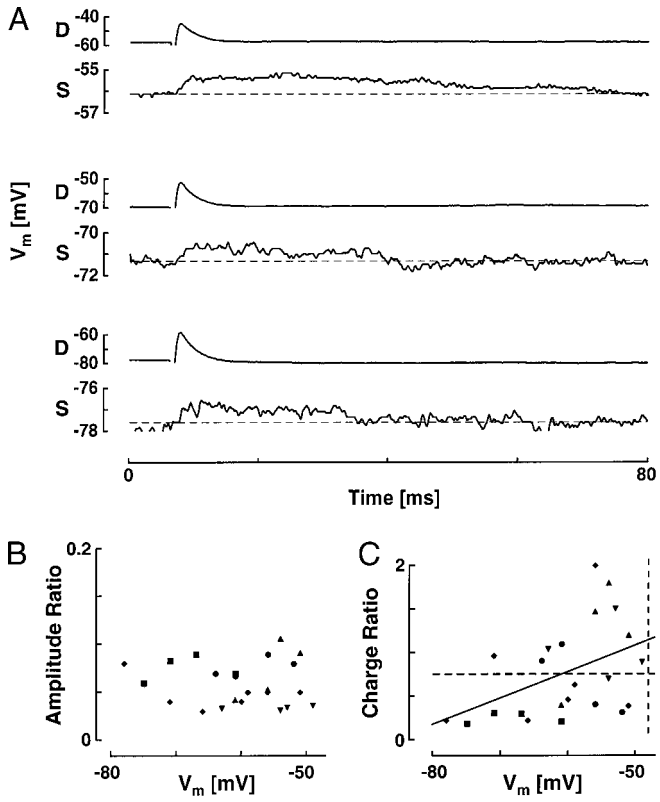

FIG. 6. Voltage-dependent EPSP efficacy. *A*: dendritic (D) and somatic (S) EPSPs generated at the dendrite by a dynamic current-clamp at 3 membrane voltages, −56, −71, and −78 mV, respectively. *B* and *C*: scatter graphs of EPSP peak amplitude (*B*) and charge (*C*) ratio in relation to membrane potential from 5 cells. The straight line in *C* was obtained by linear regression (Pearson's $r = 0.44$, $P < 0.04$). The horizontal dashed line corresponds to the mean k_{12}, i.e., the expected average electrotonic charge transfer. The vertical dashed line indicates the average action potential threshold in these cells. Data from individual cells in *B* and *C* are symbol coded.

DISCUSSION

The main findings of this study are *1*) that synaptic charge transfer from dendrite to soma is voltage-dependent, whereas the transfer of peak amplitude is not, and *2*) that at rest, voltage and charge transfer from dendrite to soma and vice versa depend on linear cable properties.

The sites of dendritic recordings in this study are relatively proximal ($X < 0.7$) compared with the total length ($L \sim 1.7$) of the apical dendrite. About 85% of all excitatory synapses are on spines (DeFelipe and Fariñas 1992; Larkman 1991b). The apical trunk of a thick layer V pyramidal cell has a spine density of 6.3/μm and a total of 3100 spines. Therefore our maximal recording distance is within the range of ~35% of all synapses on the apical trunk dendrite. However, a generalization to other synapses of similar distance on basal and oblique dendrites will have to await experimental verification. How well are synapses on spines represented by a dynamic current clamp on the stem dendrite? Recent findings suggest that spines are more likely to separate synapses biochemically rather than electrically (Svoboda et al. 1996). It is therefore reasonable to assume that our main conclusions about synaptic charge transfer are valid for synapses on spines and on shafts. This point of view is in agreement with modeling studies of synaptic conductance inputs on dendritic spines and shafts in pyramidal cells (Turner 1984).

It has recently been shown that somato-dendritic voltage attenuation can be best accounted for by a nonuniform R_m and I_h (Stuart and Spruston 1998). It is likely that I_h affects even small voltage deflections of a few millivolts, as shown by an omnipresent sag in our recordings. Therefore our estimates of R_m are unlikely to reflect strictly passive conditions. Nevertheless, the reciprocity of transfer resistances and of charge and voltage transfer holds under our resting conditions as expected for a linear system (Carnevale and Johnston 1982; Rall and Segev 1985). We conclude that within the voltage range of our observations the interplay of all open conductances still results in a linear albeit not passive membrane. A similar conclusion was drawn by studying spatial EPSP summation in hippocampal pyramidal cells (Cash and Yuste 1999).

The somatopetal current transfer properties of the apical dendrite could be satisfactorily approximated by a linear cable model. The independent estimates of L (1.7) and λ (400 μm) are in line with the morphological length of the apical trunk (~0.7 mm) in these cells (Larkman 1991a). The simple low-pass behavior of the apical dendrite agrees with similar findings from dendrites in spinal neurons (Buchanan et al. 1992). We did not find resonance phenomena in our transfer impedance measurements as described in neuroblastoma neurites (Moore et al. 1988). In neocortical pyramidal cells, somatic point impedance measurements revealed a resonance below 2.5 Hz at hyperpolarized potentials (Hutcheon et al. 1996). Because our measurements of transfer impedance were confined to resting conditions, deviations from linearity cannot be excluded at hyperpolarized membrane voltages.

Our data confirm previous experimental and modeling data (Cauller and Connors 1992; Markram et al. 1997) which demonstrated severe EPSP peak attenuation for unitary input even at moderate electrotonic distances from the soma. However, quantal current at the soma has been shown to be location independent (Jack et al. 1981; Stricker et al. 1996). This could either result from a location-scaled increase in input conductance (Stricker et al. 1996) or an appropriately balanced boosting mechanism (Cook and Johnston 1999). In our experiments, we did not scale the conductances of the dynamic current clamp for dendritic location.

Under unclamped conditions, measuring the charge arriving at the soma is not possible. However, we were able to show using double somatic recordings that the voltage integral scaled by R_N is a surprisingly precise predictor for charge estimation with accuracy in the range of 1% (well within the errors of estimating R_N). We also observed that R_N was dependent on the membrane potential. This is in agreement with the observations of Connors et al. (1982) and Stafstrom et al. (1984) in other cortical slice preparations. This finding can most likely be explained by rectification in the depolarizing direction due to I_{NaP} (Stafstrom et al. 1982) and in the hyperpolarizing direction to I_h (Spain et al. 1987).

We further obtained evidence that voltage-dependent membrane nonlinearities influence the flow of charge from a synapse to the soma. No attempt was made to assess the nature of these conductances but likely candidates for the prolongation of the EPSP above −60 mV are $I_{Na,p}$ (Stuart and Sakmann 1995) and/or I_{NMDA} (activated by ambient glutamate, Sah et al. 1989). I_h (Nicoll et al. 1993; Stuart and Spruston 1998) and/or I_A (Hoffman et al. 1997) have the potential to cause the truncation of the EPSP below −60 mV. All four currents have

been found in dendritic recordings; they activate/deactivate or inactivate in the appropriate voltage ranges and could lead to the required charge gain/loss.

What are the potential functional consequences of voltage-dependent charge transfer? Modeling studies suggest that the resting membrane voltage can be depolarized by moderate background activity of excitatory synapses (Bernander et al. 1991). From our data we predict that the additional inward current responsible for the enhanced charge transfer will increase the gain of the relationship between synaptic input and spike output under depolarized conditions. In addition, the time window for nonlinear EPSP summation will be increased for two reasons: the increase in R_N and the charge gain that is predominantly in the tail of the EPSP.

We are very grateful to Prof. S. J. Redman for carefully reading the manuscript and for excellent advice. We thank Prof. R. J. Douglas, Dr. M. Carandini, and dipl. phys. A. Kern for help with the design, implementation, and analysis of the chirps and stimulating discussions. We are indebted to Dr. A. I. Cowan for experimental support with the double somatic recordings.

This work was supported by Swiss National Science Foundation Schwerpunk Programm Biotechnologie Grants 5002-242787 and 50-52085-97.

REFERENCES

AGMON-SNIR H AND SEGEV I. Signal delay and input synchronization in passive dendritic structures. *J Neurophysiol* 70: 2066–2085, 1993.

AHMED B, ANDERSON JC, DOUGLAS RJ, MARTIN KAC, AND WHITTERIDGE D. Estimates of the net excitatory currents evoked by visual stimulation of identified neurons in cat visual cortex. *Cereb Cortex* 8: 462–476, 1998.

AMITAI Y, FRIEDMAN A, CONNORS BW, AND GUTNICK MJ. Regenerative activity in apical dendrites of pyramidal cells in neocortex. *Cereb Cortex* 3: 26–38, 1993.

BERNANDER Ö, DOUGLAS RJ, MARTIN KAC, AND KOCH C. Synaptic background activity influences spatiotemporal integration in single pyramidal cells. *Proc Natl Acad Sci USA* 88: 11569–11573, 1991.

BUCHANAN JT, MOORE LE, HILL R, WALLÉN P, AND GRILLNER S. Synaptic potentials and transfer functions of lamprey spinal neurons. *Biol Cybern* 67: 123–131, 1992.

BUTZ EG AND COWAN JD. Transient potentials in dendritic systems of arbitrary geometry. *Biophys J* 14: 661–689, 1974.

CARNEVALE NT AND JOHNSTON D. Electrophysiological characterization of remote chemical synapses. *J Neurophysiol* 47: 606–621, 1982.

CASH SS AND YUSTE R. Linear summation of excitatory inputs by CA1 pyramidal neurons. *Neuron* 22: 383–394, 1999.

CAULLER LJ AND CONNORS BW. Functions of very distal dendrites: Experimental and computational studies of layer I synapses on neocortical pyramidal cells. In: *Single Neuron Computation*, edited by McKenna T, Davis J, and Zornetzer SF. San Diego, CA: Academic, 1992, p. 199–229.

CONNORS BW AND GUTNICK MJ. Intrinsic firing patterns of diverse neocortical neurons. *Trends Neurosci* 13: 99–104, 1990.

CONNORS BW, GUTNICK MJ, AND PRINCE DA. Electrophysiological properties of neocortical neurons in vitro. *J Neurophysiol* 48: 1302–1320, 1982.

COOK EP AND JOHNSTON D. Voltage-dependent properties of dendrites that eliminate location-dependent variability of synaptic input. *J Neurophysiol* 81: 535–543, 1999.

CURTIS HJ AND COLE KS. Transverse electric impedance of the squid giant axon. *J Gen Physiol* 21: 757–765, 1938.

DEFELIPE J AND FARIÑAS I. The pyramidal neuron of the cerebral cortex: morphological and chemical characteristics of the synaptic inputs. *Prog Neurobiol* 39: 563–607, 1992.

DEISZ RA, FORTIN G, AND ZIEGLGÄNSBERGER W. Voltage dependence of excitatory postsynaptic potentials of rat neocortical neurons. *J Neurophysiol* 65: 371–382, 1991.

DODT H-U AND ZIEGLGÄNSBERGER W. Visualizing unstained neurons in living brain slices by infrared DIC-videomicroscopy. *Brain Res* 537: 333–336, 1990.

DOUGLAS RJ, KOCH C, MAHOWALD M, MARTIN KAC, AND SUAREZ HH. Recurrent excitation in neocortical circuits. *Science* 269: 981–985, 1995.

FORTI L, BOSSI M, BERGAMASCHI A, VILLA A, AND MALGAROLI A. Loose-patch recordings of single quanta at individual hippocampal synapses. *Nature* 388: 874–878, 1997.

HOFFMAN DA, MAGEE JC, COLBERT CM, AND JOHNSTON D. K^+ channel regulation of signal propagation in dendrites of hippocampal pyramidal neurons. *Nature* 387: 869–875, 1997.

HOLMES WR, SEGEV I, AND RALL W. Interpretation of time constant and electrotonic length estimates in multicylinder or branched neuronal structures. *J Neurophysiol* 68: 1401–1420, 1992.

HUGUENARD JR, HAMILL OP, AND PRINCE DA. Sodium channels in dendrites of rat cortical pyramidal neurons. *Proc Natl Acad Sci USA* 86: 2473–2477, 1988.

HUTCHEON B, MIURA RM, AND PUIL E. Subthreshold membrane resonance in neocortical neurons. *J Neurophysiol* 76: 683–697, 1996.

JACK JJB, REDMAN SJ, AND WONG K. The components of synaptic potentials evoked in cat spinal motoneurones by impulses in single group Ia afferents. *J Physiol (Lond)* 321: 65–96, 1981.

KIM HG AND CONNORS BW. Apical dendrites of the neocortex: correlation between sodium- and calcium-dependent spiking and pyramidal cell morphology. *J Neurosci* 13: 5301–5311, 1993.

LARKMAN AU. Dendritic morphology of pyramidal neurones of the visual cortex of the rat: I. Branching patterns. *J Comp Neurol* 306: 307–319, 1991a.

LARKMAN AU. Dendritic morphology of pyramidal neurones of the visual cortex of the rat: III. Spine distributions. *J Comp Neurol* 306: 332–343, 1991b.

LARKMAN AU, MAJOR G, STRATFORD KJ, AND JACK JJB. Dendritic morphology of pyramidal neurones of the visual cortex of the rat: IV. Electrical geometry. *J Comp Neurol* 323: 137–152, 1992.

MARKRAM H, LÜBKE J, FROTSCHER M, ROTH A, AND SAKMANN B. Physiology and anatomy of synaptic connections between thick tufted pyramidal neurones in the developing rat neocortex. *J Physiol (Lond)* 500: 409–440, 1997.

MARKRAM H AND SAKMANN B. Calcium transients in dendrites of neocortical neurons evoked by single subthreshold excitatory postsynaptic potentials via low-voltage-activated calcium channels. *Proc Natl Acad Sci USA* 91: 5207–5211, 1994.

MOORE LE, YOSHII K, AND CHRISTENSEN BN. Transfer impedances between different regions of branched excitable cells. *J Neurophysiol* 59: 689–705, 1988.

NICOLL A, LARKMAN A, AND BLAKEMORE C. Modulation of EPSP shape and efficacy by intrinsic membrane conductances in rat neocortical pyramidal neurons in vitro. *J Physiol (Lond)* 468: 693–710, 1993.

RALL W AND SEGEV I. Space-clamp problems when voltage clamping branched neurons with intracellular microelectrodes. In: *Voltage and Patch Clamping With Microelectrodes*, edited by Smith TG Jr, Lecar H, Redman SJ, and Gage PW. Bethesda, MD: American Physiological Society, 1985, p. 191–215.

ROBINSON HPC AND KAWAI N. Injection of digitally synthesized synaptic conductance transients to measure the integrative properties of neurons. *J Neurosci Meth* 49: 157–165, 1993.

SAH P, HESTRIN S, AND NICOLL RA. Tonic activation of NMDA receptors by ambient glutamate enhances excitability of neurons. *Science* 246: 815–818, 1989.

SCHWINDT PC AND CRILL WE. Equivalence of amplified current flowing from dendrite to soma measured by alteration of repetitive firing and by voltage clamp in layer 5 pyramidal neurons. *J Neurophysiol* 76: 3731–3739, 1996.

SCHWINDT PC AND CRILL WE. Synaptically evoked dendritic action potentials in rat neocortical pyramidal neurons. *J Neurophysiol* 79: 2432–2446, 1998.

SHARP AA, O'NEIL MB, ABBOTT LF, AND MARDER E. Dynamic clamp: computer-generated conductances in real neurons. *J Neurophysiol* 69: 992–995, 1993.

SPAIN WJ, SCHWINDT PC, AND CRILL WE. Anomalous rectification in neurons from cat sensorimotor cortex in vitro. *J Neurophysiol* 57: 1555–1576, 1987.

STAFSTROM CE, SCHWINDT PC, CHUBB MC, AND CRILL WE. Properties of persistent sodium conductance and calcium conductance of layer V neurons from cat sensorimotor cortex in vitro. *J Neurophysiol* 53: 153–170, 1985.

STAFSTROM CE, SCHWINDT PC, AND CRILL WE. Negative slope conductance due to a persistent subthreshold sodium current in cat neocortical neurons in vitro. *Brain Res* 236: 221–226, 1982.

STAFSTROM CE, SCHWINDT PC, FLATMAN JA, AND CRILL WE. Properties of subthreshold response and action potential recorded in layer V neurons from cat sensorimotor cortex in vitro. *J Neurophysiol* 52: 244–263, 1984.

STRICKER C, FIELD AC, AND REDMAN SJ. Statistical analysis of amplitude fluctuations in EPSCs evoked in rat CA1 pyramidal neurones in vitro. *J Physiol (Lond)* 490: 419–441, 1996.

STUART GJ AND SAKMANN B. Active propagation of somatic action potentials into neocortical pyramidal cell dendrites. *Nature* 367: 69–72, 1994.

STUART GJ AND SAKMANN B. Amplification of EPSPs by axosomatic sodium channels in neocortical pyramdial neurons. *Neuron* 15: 1065–1076, 1995.

STUART GJ AND SPRUSTON N. Determinants of voltage attenuation in neocortical pyramidal neuron dendrites. *J Neurosci* 18: 3501–3510, 1998.

SVOBODA K, TANK DW, AND DENK W. Direct measurement of coupling between dendritic spines and shafts. *Science* 272: 716–719, 1996.

TURNER DA. Conductance transients onto dendritic spines in a segmental cable model of hippocampal neurons. *Biophys J* 46: 85–96, 1984.

ULRICH D AND HUGUENARD JR. γ-aminobutyric acid type B receptor-dependent burst-firing in thalamic neurons: a dynamic clamp study. *Proc Natl Acad Sci USA* 93: 13245–13249, 1996.

ULRICH D AND HUGUENARD JR. $GABA_A$-receptor-mediated rebound burst firing and burst shunting in thalamus. *J Neurophysiol* 78: 1748–1751, 1997.